JOURNAL OF MATERIALS SCIENCE 31 (1996) 731–740

Toughness and microscopic fracture mechanisms of unfilled and short-glass-fibre-filled poly(cyano arylether)

N.S. CHOI, K. TAKAHASHI
Research Institute for Applied Mechanics, Kyushu University, Kasuga, Fukuoka 816 Japan

Fracture mechanisms of an advanced high-strength thermoplastic poly(cyano arylether) (PCAE) and its short-glass-fibre (SGF)-reinforced composites have been studied in relation to toughnesses K_c and J_c. Test temperatures were 23 and 100 °C. Reflected and transmitted optical observations were combined with scanning electron microscopy for the fractographic investigation. For unreinforced PCAE tested at 100 °C, the damage area in front of a notch becomes fairly large in size and consists of numerous tensile microfailures around the local plastic yielding zone, as compared with that tested at 23 °C. This resulted in a substantial improvement of K_c and a big increase in J_c. Filling fibres, however, produced both toughening and anti-toughening results: effects of fibre spanning, pull-out and bridging across the local plastic failure zone and zigzag propagation of fracture due to fibre filling, improved the toughness. However, adhesive failure at the fibre–matrix interface, tensile microcleavage at the fibre ends and straightforward fracture in the skin layer, considerably diminished the values of K_c and J_c, except for the trend of K_c at 23 °C.

1. Introduction

Thermoplastic polymers have been increasingly utilized as matrices of high-performance composites because they have advantages of thermoformability, recyclability and weldability [1]. In particular, short-fibre-reinforced thermoplastics (SFRTP) of high-cost performance have extensively been used in industry. In comparison to continuous fibre-reinforced composites, however, SFRTP do not have so good fracture strengths and toughnesses because the stress concentration at the fibre ends allows failure to be initiated easily [2–10]. Fracture mechanisms of SFRTP employing such matrix polymers as polypropylene (PP) [3–5], poly(ether ether ketone) (PEEK) [6, 7], polyamide (PA) [8–10] and polyethylene terephthalate (PET) [10, 11] have been investigated in recent years to improve their mechanical properties.

Poly(cyano arylether) (PCAE) is one of the advanced high-strength thermoplastics originally developed by Idemitzu Kosan Co. It is a crystalline polymer having the cyano-nitrile radical appended to the aromatic ring and showing superior tensile strength (127 MPa at 23 °C) [12], high glass transition temperature ($T_g \approx 145$ °C) [12, 13] and heat distortion temperature ($T_{hd} \approx 165$ °C) [13]. The molecular structure is

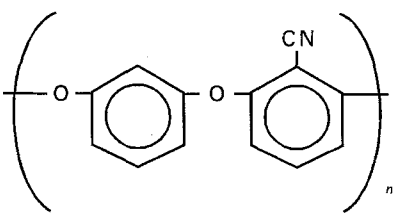

Nishitani *et al.* [14] studied the influence of the notch tip radius on the fracture strength of short fibre-reinforced (SFR) PCAE on the basis of linear elastic mechanics concepts. Recently, Nagoh *et al.* [12] reported testing temperature effects on tensile strength and fracture toughness of unreinforced (UR) and SFR-PCAE: The UR-PCAE exhibited superior performance in stiffness, glass transition temperature and tensile strength as compared with PEEK [15]. However, SFR- and UR-PCAE below 50 °C showed low fracture toughness, J_c. At 100 °C, on the other hand, toughness was significantly increased.

The purpose of the present work was to investigate fracture mechanisms in conjunction with toughness of UR- and short-glass-fibre reinforced (SGFR) PCAE specimens. Reflected and transmitted optical observations, in combination with scanning electron microscopy, were used for fractographic examinations. A thin sectioning technique [16] was utilized for the optical microscopy. Particular attention was given to the influence of test temperature and fibre weight fraction on the fracture mechanisms.

2. Experimental procedure

2.1. Composites

Injection-moulded UR- and SGFR-PCAE plates (80 mm × 80 mm × 3 mm) were prepared for this investigation. The E-glass fibres of 13 μm diameter were surface-treated with an amino-silane coupling agent and a urethane sizing agent to ensure good adhesion with the matrix. The fibre weight fractions were 10% and 30%. The pre-compounded pellets were melted

0022–2461

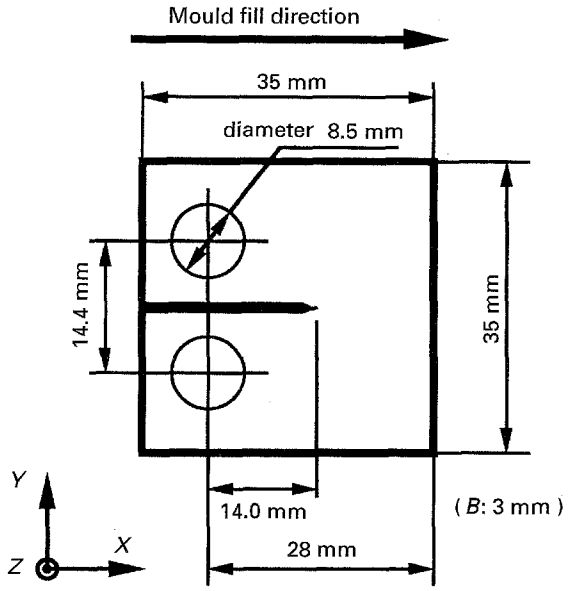

Figure 1 Geometry of compact tension specimen and mould-fill direction.

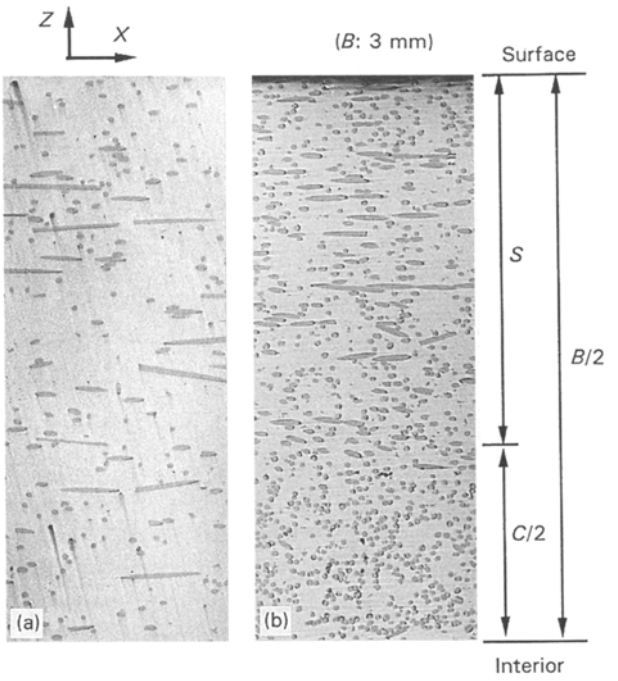

Figure 2 Orientation of short fibres in specimens; (a) SGF 10 wt %-PCAE, (b) SGF 30 wt %-PCAE.

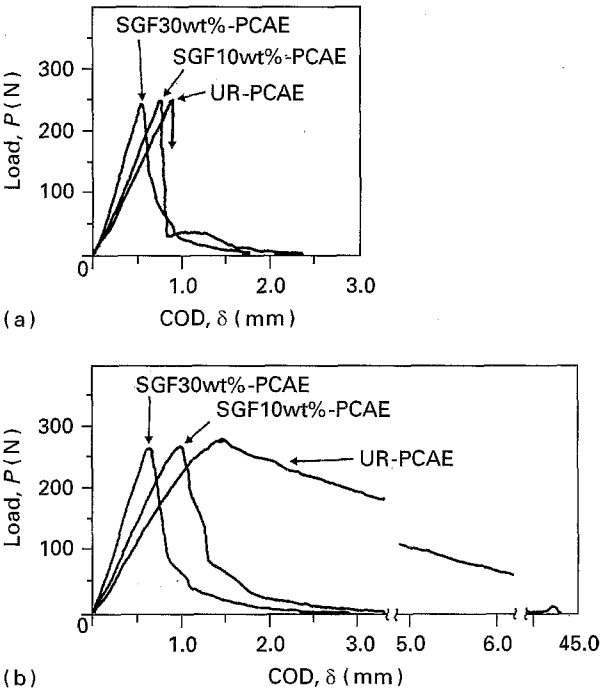

Figure 3 Typical load–displacement curves of UR- and SGFR-PCAE specimens at (a) 23 °C, and (b) 100 °C.

in a cylinder heated to 340 °C and were injected into end-gated plaque-shaped moulds at 230 °C using a conventional injection-moulding machine. Compact tension (CT) specimens with the geometry shown in Fig. 1 were machined from the central part of the plates. Specimens were notched parallel to the mould-fill direction (MFD). The machining and notching were performed with a diamond saw. The notch was sharpened with a fresh razor blade to form an artificial crack tip (ACT). Fig. 2a and b show short fibres optically observed on polished surfaces near ACT of SGF 10 wt %- and SGF 30 wt %-PCAE specimens, respectively. Fibres were considerably aligned in the MFD for SGF 10 wt %-PCAE. SGF 30 wt %-PCAE, however, had a skin and core layered [10, 17] structure: fibres were primarily aligned along the MFD in the skin layer, while those in the inner core layer were oriented perpendicular to the MFD. Fibre lengths in SGF 10 wt % specimens had a distribution in a range of 30–620 μm with a peak at about 170 μm, while those in SGF 30 wt % had a peak at about 146 μm in a range of 20–540 μm. The PCAE resin had a crystallinity [13] of about 30% which was determined by differential scanning calorimetric (DSC) analysis. The diameter of the spherulites was less than 1 μm, and they were scarcely visible under a polarizing transmission optical microscope.

2.2. Fracture toughness testing

The compact tension specimens described above were loaded with a crosshead speed of 0.5 mm min^{-1}. Test temperatures, T, were 23 and 100 °C, where fracture behaviour for UR-PCAE was brittle and ductile, respectively [12] (see Fig. 3). Five specimens were tested for each experimental condition.

From the load–load point displacement (P–δ) curves, the maximum load was considered to be the critical load corresponding to the crack initiation point, P_c. Values of the critical stress intensity factor, K_c, were obtained from the Equation [18]

$$K_c = \frac{P_c}{BW} a^{1/2} Y(a/W) \quad (1)$$

where B is the specimen thickness (3 mm), W is the specimen width (28 mm), a is the initial crack length (14.0 ± 0.2 mm) and $Y(a/W)$ is the geometrical correction factor. K_c is based on an elastic fracture criterion. On the other hand, the J-integral postulates elastic–plastic fracture and its critical value, J_c, was determined using the equation suggested by

Rice [19]

$$J_c = \frac{2U_c}{B\,(W-a)} \quad (2)$$

where U_c is the area bounded by the P–δ curve up to the crack initiation point and the corresponding δ axis.

2.3. Microscopic fracture examination

Specimens were unloaded from loaded states. Thinning was essential for optical observation under transmitted light because specimens were not optically transparent. Thin sections were prepared by lapping the specimens to a thickness of 20–30 μm and then polishing with buff and abrasive alumina powder (0.05 μm diameter). The sections were examined using a polarized optical microscope under reflected and transmitted light [16]. Fracture surface investigation was also performed with a scanning electron microscope (SEM) as a complement to the optical fractography.

3. Results and discussion

3.1. Fracture toughness

Fig. 3 shows typical P–δ curves of UR, SGF 10 wt % and SGF 30 wt % specimens. At 23 °C (see Fig. 3a), the three specimens exhibited almost linear relationships between P and δ up to the peak points, although the stiffness increased with increasing fibre weight fraction, W_f. At 100 °C, on the other hand, UR-PCAE was ductile as shown in Fig. 3b. With increasing W_f compliance and δ at the maximum load greatly diminished. The increase in ductility in UR-PCAE at 100 °C influenced only slightly the ductility of SGF 30 wt %-PCAE.

Fracture toughness of the PCAE specimens as a function of W_f is shown in Fig. 4. An averaged value of K_c for UR-PCAE was about 4.2 MPam$^{1/2}$ at 23 °C and almost unchanged with W_f as seen in Fig. 4a. At 100 °C, in contrast, values of K_c for UR-PCAE increased 16% and the composites exhibited a monotonic decrease in K_c; specimens of SGF 30 wt %-PCAE had values only 6% higher than those at 23 °C.

Fig. 4b presents values of J_c for PCAE specimens. At 23 °C, specimens showed a slight decrease in J_c with increasing W_f: averaged values for UR- and SGF 30 wt %-PCAE were 3.8 kJ m^{-2} and 3.2 kJ m^{-2}. At 100 °C, however, J_c was greatly lowered as W_f increased: the value of J_c for UR-PCAE (9.6 kJ m^{-2}) was about 2.3 times as large as that at 23 °C. SGF 10 wt % and 30 wt %-PCAE exhibited values of about 6.3 and 4.3 kJ m^{-2}, respectively.

Concluding, UR-PCAE at 100 °C revealed higher values in both K_c and J_c than those at 23 °C. Ductility of PCAE resin is considerably affected by the temperatures [12] and this influences toughness. However, SGFR-PCAE showed a smaller increase in the toughnesses at high temperature. These less effective results should, therefore, be more closely involved in the fracture mechanisms for UR- and so also for SGFR-PCAE.

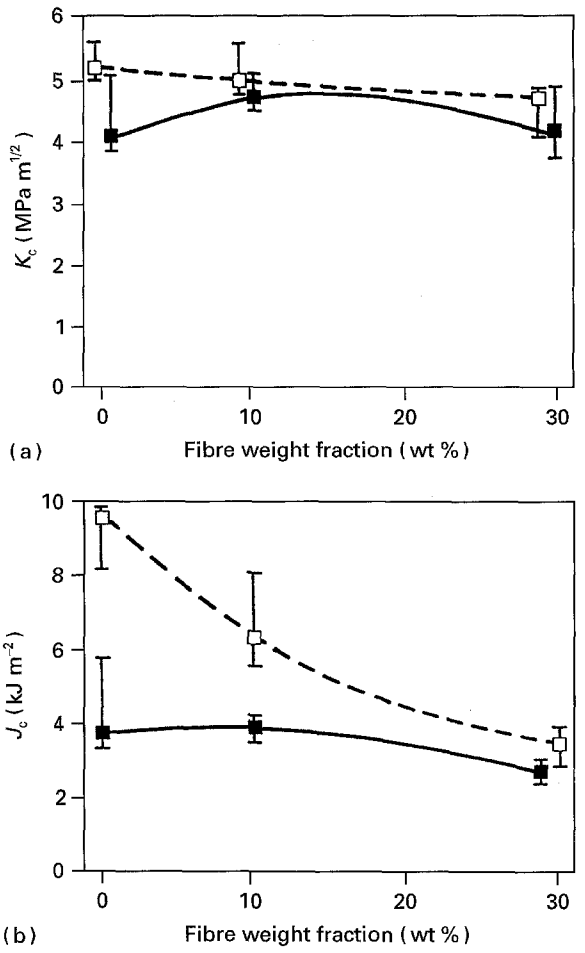

Figure 4 (a) Critical stress intensity factor, K_c, and (b) critical J-integral, J_c, of UR-and SGFR-PCAE specimens. (■) 23 °C, (□) 100 °C.

3.2. Fracture mechanisms for UR-PCAE

Fig. 5a shows a scanning electron micrograph of a fracture surface in a low-speed stable fracture zone near the artificial crack tip (ACT) for UR-PCAE tested at 23 °C. The slow fracture propagated about 200–300 μm from the ACT and thereafter changed to a fast fracture. It is indicated that an elliptical front was formed at the crack tip. The fracture left a trace of a stretched zone, approximately 30 μm in length, near the ACT. The matrix at the ACT underwent local plastic deformation under tensile loading, inducing crack tip blunting ("normal yielding"). The plastic deformation process of the matrix might have been accompanied by the formation of secondary cavities and microvoids, crazing or craze-like failure [20]. Those microfailures must have been initiated at some inhomogeneities in the local plastic yielding zone, where they formed equiaxed dimple-like patterns. Similar patterns are observed on fracture surfaces of polystyrene (PS) [21] and a thick PEEK [27]. The size of the dimple-like patterns near the ACT was almost the same as the length of the stretched zone. Further, a transmitted optical micrograph (Fig. 5b) taken from a thin section cut perpendicular to the fracture surface, revealed that this surface was macroscopically flat and a few branched tensile failure facets were formed underneath it. Local plastic flows may also have occurred in the failure facets.

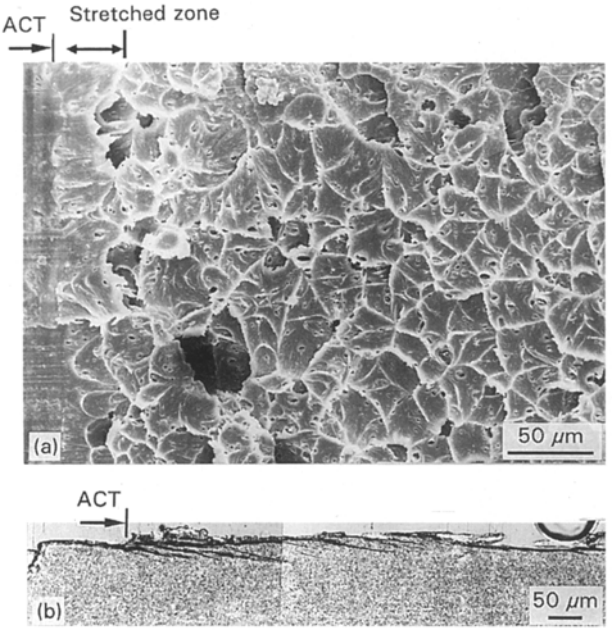

Figure 5 (a) Scanning electron micrograph taken from the fracture surface of a UR-PCAE specimen tested at 23 °C; (b) a transmitted optical micrograph taken from a thin specimen sectioned vertical to the fracture surface in (a).

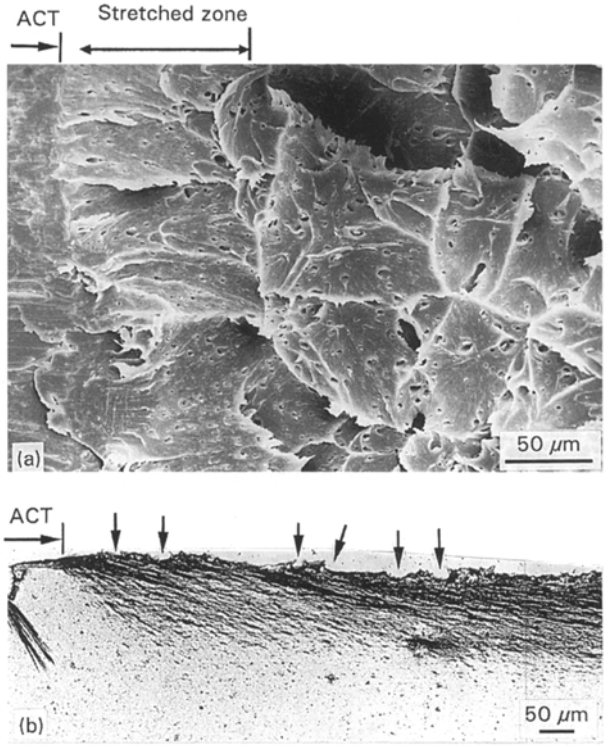

Figure 6 (a) Scanning electron micrograph taken from a fracture surface of a UR-PCAE specimen loaded at 100 °C; (b) a transmitted light micrograph obtained from a thin specimen sectioned vertical to the fracture surface in (a).

Fracture surfaces for UR-PCAE tested at 100 °C observed in a way similar to Fig. 5, are shown in Fig. 6. The length of stretched zone seen in Fig. 6a was approximately 87 μm, about three times as large as that at 23 °C. The dimple-like patterns were also formed after the matrix at the ACT was locally stretched, their sizes were equivalent to the length of the

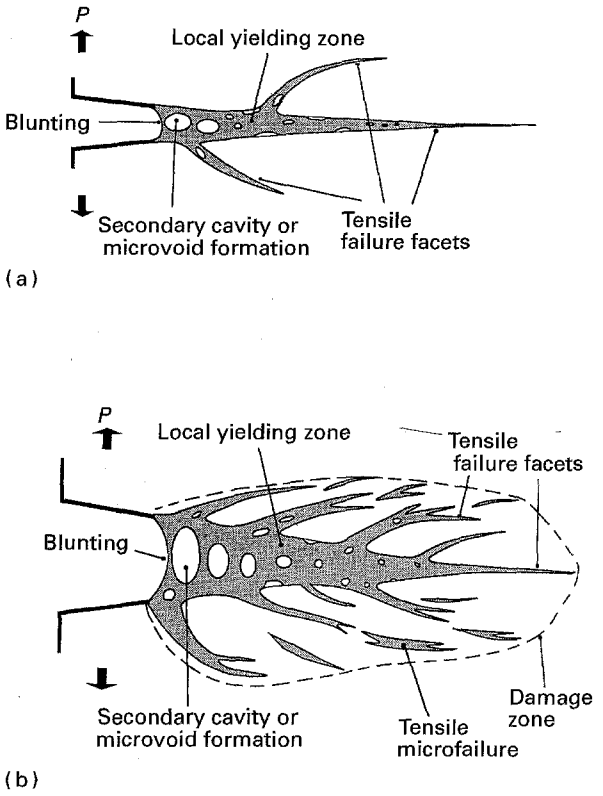

Figure 7 Schematic illustration showing fracture mechanisms of UR-PCAE at (a) 23 °C and (b) 100 °C.

stretched zone. The number of patterns became smaller compared with that at 23 °C. The patterns resulted from the growth and coalescence of cavities as shown by arrows in Fig. 6b. Shear lips were rarely observed at the edges of the fracture surface, while underneath this surface, numerous tensile microfailures were visible. The cavitation and microfailure formation around the ACT must have required much energy during loading of the specimens. The fracture proceeded in a stable manner until the final separation occurred.

Failure mechanisms for UR-PCAE at 23 and 100 °C are presented schematically in Fig. 7a and b, respectively. While UR-PCAE at 23 °C generated a few branched tensile failure facets, it exhibited at 100 °C formation of many microfailures around the main cracking, as well as the large growth of cavities in the failure facets.

3.3. Fracture mechanisms for SGFR-PCAE

Fig. 8 shows typical polarized optical micrographs taken from a thin section of an SGF 10 wt %-PCAE specimen tested at 23 °C. The section was obtained from a specimen deformed up to the maximum load, i.e. just before the catastrophic fracture. When examined under reflected light (Fig. 8a), slim figures of tensile microfailure in the matrix, fibre–matrix interfacial microcracking and/or debonding at several fibre ends, were observed in front of the ACT. The main cracking was only slightly visible at the notch tip. Thus, debonding and matrix microfailure seemed to precede the main cracking. When the same section was viewed under transmitted light (Fig. 8b), however, a damage

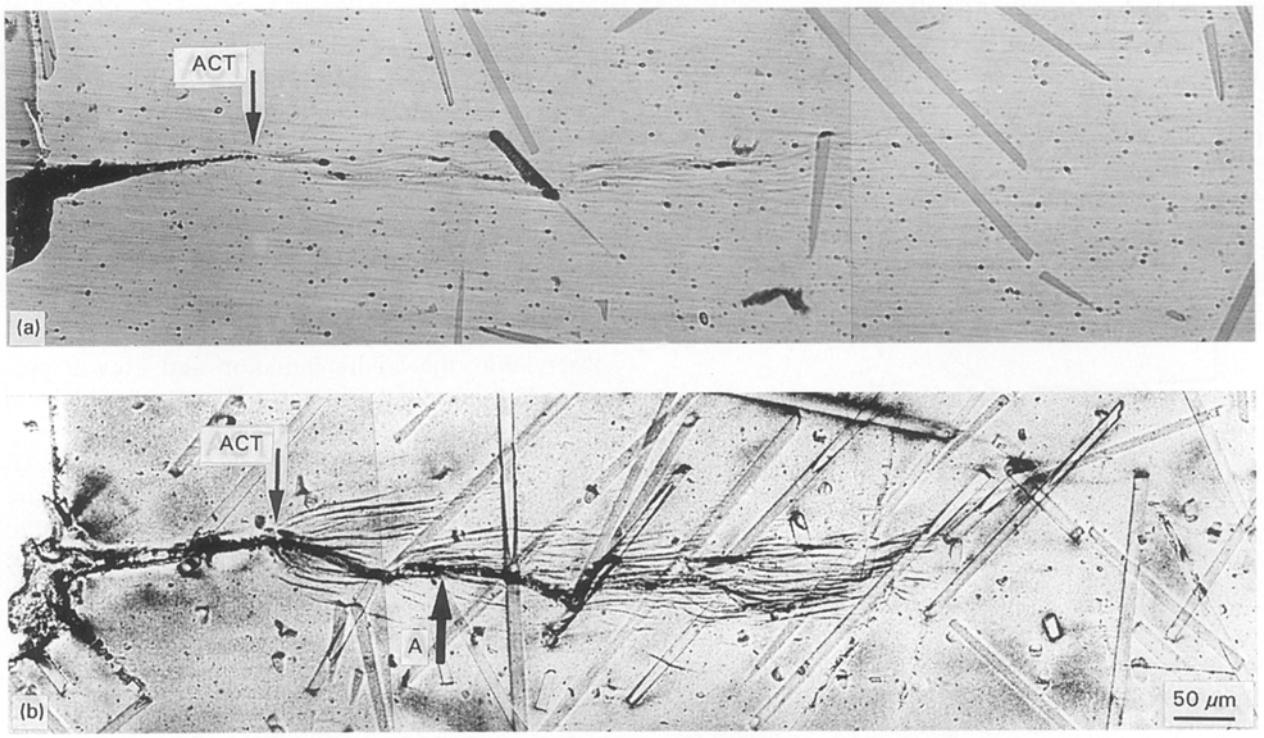

Figure 8 Polarized optical micrographs of a SGF 10 wt %-PCAE specimen which was loaded just prior to the catastrophic fracture at 23 °C under (a) reflected and (b) transmitted light.

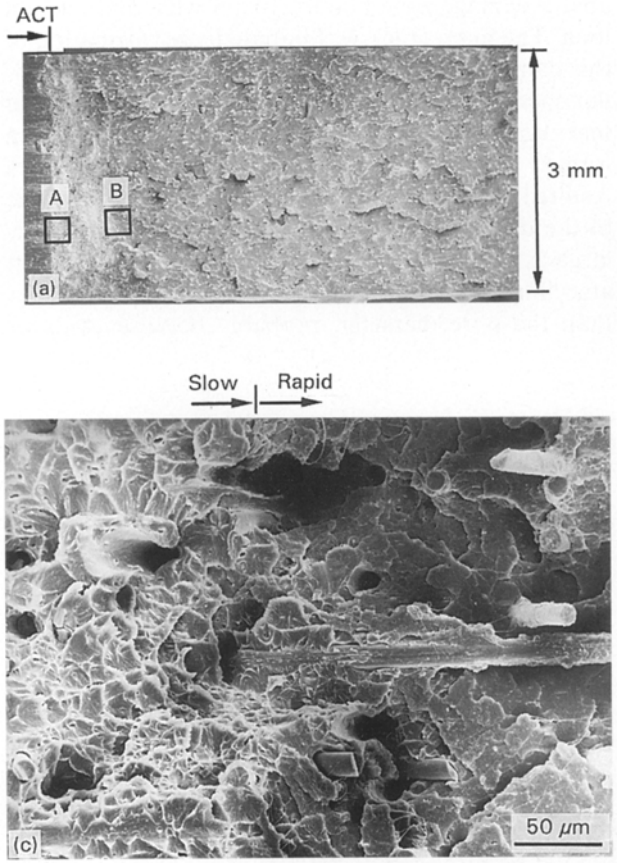

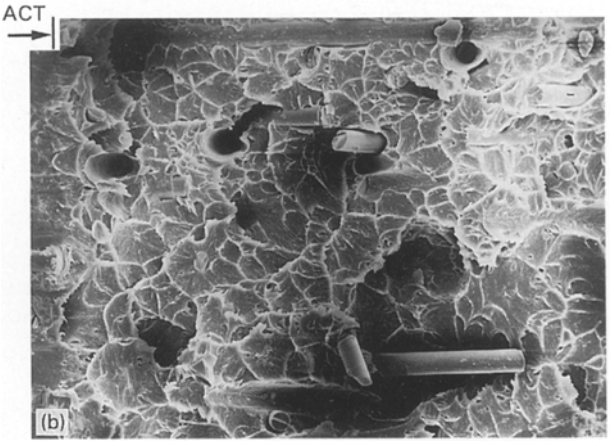

Figure 9 Scanning electron micrographs of a fracture surface of a SGF 10 wt %-PCAE specimen tested at 23 °C: (a) overall view, (b, c) are enlarged pictures of areas A and B in (a).

zone about 115 μm wide and 570 μm long was obvious ahead of the ACT. A multitude of branched tensile failure facets and fibre breakages had already formed. Repair of a similar failure in a different specimen by a thermal treatment suggests that most of the matrix microfailures were not in an opened or cracked state, but in a "finely opened" or crazed state. This may be why the damage zone was almost invisible under reflected light. A band of the local plastic yielding (arrow A) of a nearly tensile mode was seen to extend about 420 μm in advance of the main cracking. This local yielding followed the pathways which had been spanned by many reinforcing fibres. Fibre breakage and/or fibre pull-out from the matrix took place together with the local yielding, and the matrix seemed to be separated in a rather ductile manner.

As suggested by an analysis of the amplitude distribution for acoustic emission waves from the damage zone of SFRTP [22], fibre breakage ahead of the crack tip might be a prerequisite for the crack initiation. A scanning electron micrograph taken from the fracture surface of a similar specimen is presented in Fig. 9. Fig. 9a shows an overall view of the surface.

The stable fracture with the elliptical front proceeded about 560 μm from the ACT. Similar to the case of UR-PCAE, a stretched zone and numerous dimple-like patterns were formed in the stable fracture region (Fig. 9b). Broken and pulled-out fibres were also observed in this region. There was little matrix debris adhering to the surfaces of the pulled-out fibres. This indicates that bonding between fibres and matrix was not strong enough, thus fibre pull-out proceeded with interfacial adhesive failure. In the fast-fracture region, the interfacial strength seemed to be greater than the matrix strength, as seen in Fig. 9c, which indicates that matrix debris adhered to fibre surfaces. No dimple patterns were discernible in this region. The cohesive failure at the matrix near the interface took place in the process of the fibre pull-out. Based on the above observation, the failure initiation and growth processes in front of the ACT are schematically shown in Fig. 10a and b, respectively.

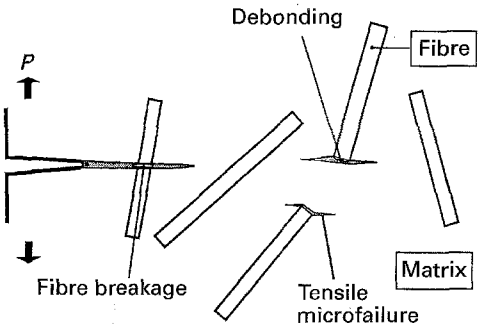

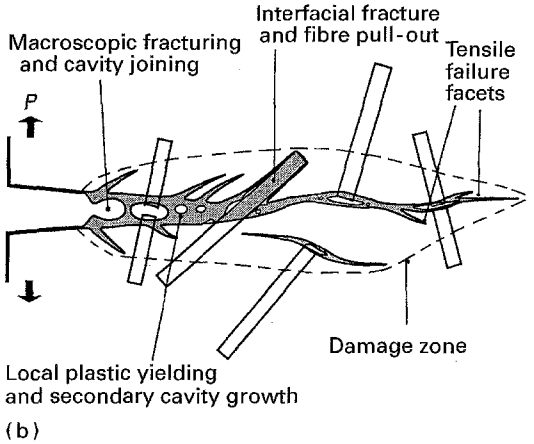

Figure 10 Schematic illustration showing fracture mechanisms of SGFR-PCAE at 23 °C: (a) failure initiation ahead of the artificial crack tip; (b) evolution of the macroscopic fracture.

Fracture processes in an SGF 10 wt %-PCAE specimen tested at 100 °C were also examined under reflected (Fig. 11a) and transmitted light (Fig. 11b) in a similar way. The specimen was loaded up to about the maximum. A local plastic yielding under a stretching progressed for a length of about 650 μm from the ACT, forming a band containing fibre breakage, debonding between fibre and matrix, fibre pull-out and microcleavage or yielding in matrix (Fig. 11a). As seen in Fig. 11b, however, numerous tensile microfailures were generated in the matrix and/or at the fibre ends near the local yielding band. The microfailures were grown around the local yielding band, which generated a damage zone about 210 μm wide and 890 μm long. The main crack was initiated after formation of this damage zone. A typical fracture surface of a similar specimen is shown in Fig. 12. A stretched zone of matrix is seen at the ACT. Large dimple patterns were formed at sites of the fibre ends, which must have resulted from large void growth at these ends. The size of the dimple patterns was, on average, 2.6 times as large as that at 23 °C in Fig. 9b. Open holes were left after fibres were pulled out and their sizes were larger than the fibre diameter, probably because voids or

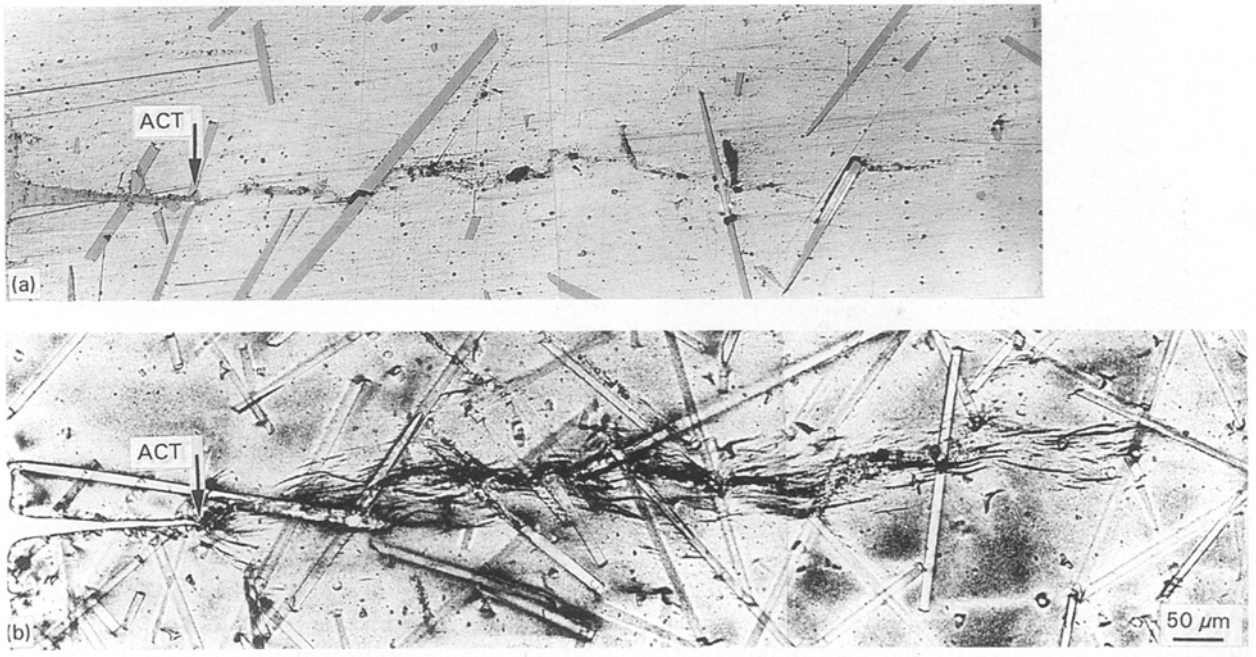

Figure 11 Polarized optical micrographs of a SGF 10 wt %-PCAE specimen which was loaded just prior to the maximum at 100 °C under (a) reflected and (b) transmitted light.

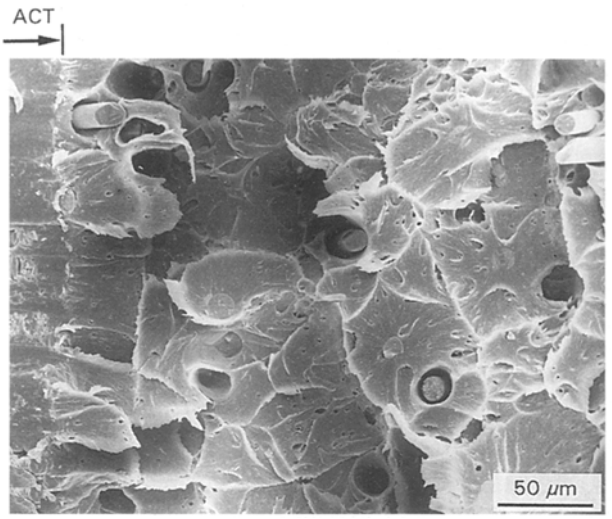

Figure 12 Scanning electron micrograph of a fracture surface of a SGF 10 wt %-PCAE specimen tested at 100 °C.

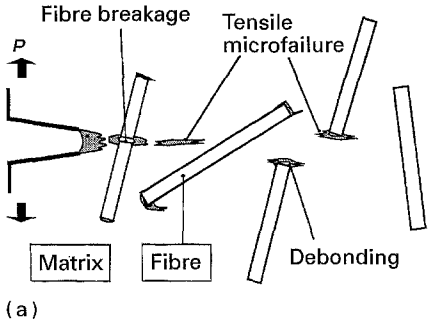

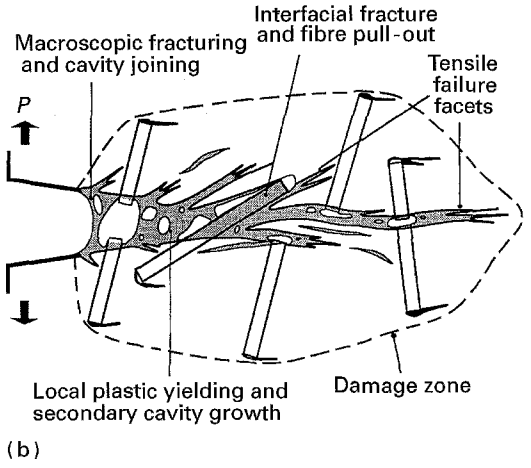

Figure 13 Schematic illustration showing fracture mechanisms of SGFR-PCAE at 100 °C: (a) failure initiation ahead of the artifical crack tip; (b) evolution of the macroscopic fracture.

cavities around the fibre ends grew during the process of specimen stretching. Little matrix fracture debris remained on the fibre surfaces, which was similar to the result in Fig. 9b. The stable fracture proceeded until the final separation. The fracture mechanisms at the damage initiation and just before the macroscopic fracturing are schematically presented in Fig. 13a and b, respectively. Compared with the case at 23 °C, local plastic failure and secondary cavities grew much more

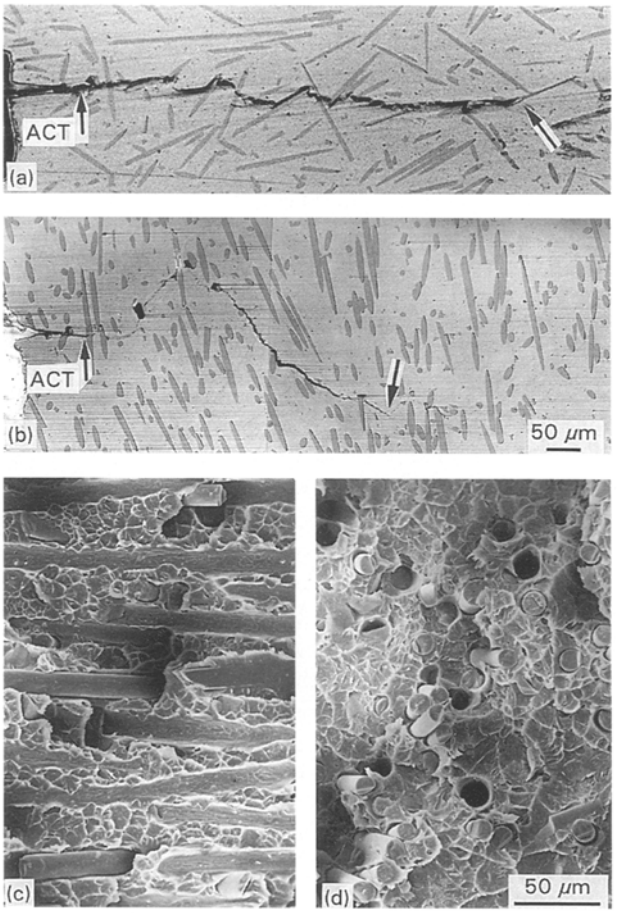

Figure 14 Reflected optical micrographs of (a) the skin and (b) the core layers of a SGF 30 wt %-PCAE specimen which was loaded just after the maximum load at 23 °C. The specimen was polished for the X–Y plane shown in Fig. 1. (c, d) Scanning electron micrographs taken from the fracture surface of the skin and core layers, respectively.

in the heavily damaged band and numerous microfailures also took place, forming a large damaged area.

Fig. 14 presents typical photographs of fracture in SGF 30 wt %-PCAE specimens tested at 23 °C. Reflected-light micrographs taken from the skin and core layers of specimens whose load was at the maximum, are shown in Fig. 14a and b, respectively. SEM fracture surface micrographs for both layers are also presented in Fig. 14c and d. Fracture behaviour in each layer was different: the main crack progressed in a straightforward manner in the skin layer (Fig. 14a), where fibre alignment in the notch direction and adhesive interfacial failure (Fig. 14c) easily resulted in flat cleavage. In the core layer, on the other hand, the main crack propagated in a zigzag way following debonded cracks at the fibre ends (Fig. 14b). This occurred because most fibres, which were oriented perpendicular to the notch direction, became obstacles to cracking, thus inducing zigzag crack propagation or occasionally fibre breakage as observed on the fracture surface. It is shown that the crack propagation length in the core layer (see arrow in Fig. 14b) was only about 71% of that in the skin layer (arrow in Fig. 14a). A damage zone, including many branched failure facets, invisible under the reflected optical microscope, probably formed prior to the main cracking. The stable fracture prevailed over the fracture

process until the final separation. Dimple patterns were seen between fibres on the fracture surface (Fig. 14c and d). Their size was about half of that for SGF 10 wt %-PCAE at 23 °C. The large fibre concentration suppressed the growth of voids or cavities in PCAE matrix.

Fracture processes in SGF 30 wt %-PCAE specimens tested at 100 °C are presented in Fig. 15. They were studied in a way similar to those of Fig. 14. Fig. 15a and b show fracture mechanisms in the skin and core layers of a specimen loaded to about the maximum. Interfacial cleavage and voiding were generated ahead of the ACT in the skin layer through adhesive failure along the fibres, giving rise to a microscopic failure band strongly oriented in the notch direction. In the core layer, on the other hand, voiding took place at the fibre ends. A failure band was composed of microcleavages generated between the voids, which proceeded in a zigzag pattern. Length of the failure band (see arrow in Fig. 15b) was 1.5 times as large as that in the skin layer (arrow in Fig. 15a), which was the reverse of the fracture trend of specimens at 23 °C where the crack propagation length for the core layer was less than that for the skin layer. The longer failure band in the core layer is due, first, to the formation of an elliptical fracture front under three-dimensional stresses at the ACT [23], and, second, to a considerable increase in matrix ductility which resists matrix cleavage in the skin layer. A damage zone containing numerous tensile microfailures similar to the results in Fig. 11b must have been generated around the failure band. The main crack seemed to follow the failure band. Fracture surfaces for both layers are also shown in Fig. 15c and d. Dimple patterns were somewhat larger than those shown in Fig. 14 at room temperature; this resulted from growth of cavities in the matrix in advance of the main cracking.

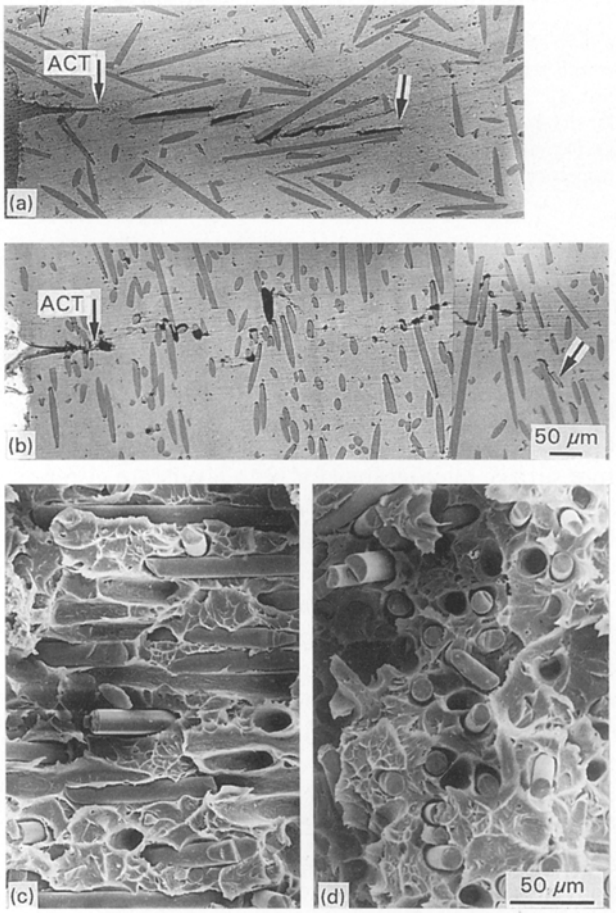

Figure 15 Reflected optical micrographs of (a) the skin and (b) the core layers of a SGF 30 wt %-PCAE specimen which was loaded just prior to the maximum load at 100 °C. The specimen was polished for the X–Y plane shown in Fig. 1. (c, d) Scanning electron micrographs of the fracture surface corresponding to the skin and core layers.

3.4. Toughening effects

Table I indicates the mechanisms responsible for the increase in toughness of UR-PCAE at 100 °C. An increase in K_c is caused by an increase in the maximum load, i.e. the strength at the ACT, whereas an increase in J_c is due to an increase in the maximum load and deformation, i.e. the absorbed energy around the ACT. In comparison with the fracture at 23 °C, UR-PCAE at 100 °C exhibited larger stretched zones and, as a result, larger dimples as illustrated in Fig. 16. The dimple patterns were generated by cavitation ahead of the ACT where local ductility was set up and influenced yielding under tensile loading. The cavities expanded during the growth of the local yielding zone. Fibrils or fibril-like structures were oriented between the cavities normal to the crack plane at the maximum load level, which should have strengthened the local plastic yielding zone [18]. Furthermore, numerous tensile microfailures were generated within a large area around the tensile failure facet. The microfailures

TABLE I Toughening factors of UR-PCAE with increasing test temperature

$T = 23\,°C \rightarrow 100\,°C$
(1) Large growth of local yielding zone and secondary cavity in the tensile failure facets (TFF)
(2) Numerous microfailures around the TFF
(3) Large area of damage zone ahead of the initial crack tip

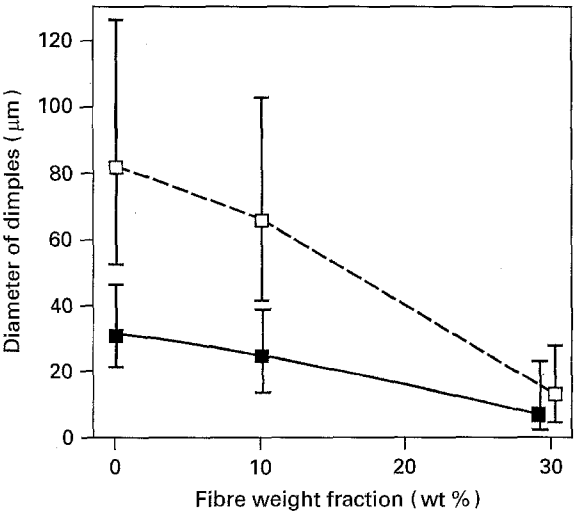

Figure 16 The average diameter of matrix dimples formed on fracture surfaces. (■) 23 °C (□) 100 °C.

TABLE II Important factors for toughening SGFR-PCAE with increasing test temperature

$T = 23°C \rightarrow 100°C$
(1) Toughening effect
The same as (1), (2) and (3) in Table I
Fibre spanning, pull-out and bridging
Zigzag fracture path in the core layer
(2) Anti-toughening effect
Adhesive failure at the fibre–matrix interface
Tensile fracture at the fibre ends
Fibre breakage-induced matrix cracking
Straightforward fracture path in the skin layer

are considered to have played an important role, firstly in dispersion and/or relief of stress concentration at the crack tip, and secondly in reduction of elastic modulus, thus increasing deformation in the damaged zone [24]. The growth of the local plastic yielding zone and formation of numerous microfailures in a large damaged area may have caused a substantial improvement in the strength and a vast increase in the absorbed energy, thus enlarging the resistance to cracking. The fracture behaviour affected the increasing trends of K_c and J_c for UR-PCAE at 100 °C as shown in Fig. 4.

Table II shows influential fracture mechanisms for toughening SGFR-PCAE. The matrix fracture mechanisms stated above must raise the toughness of SGFR-PCAE with increasing temperature. However, fibre concentration had both toughening and anti-toughening effects: fibre spanning, pull-out and bridging across the local plastic yielding and failure band, and taking a zigzag fracture path may have improved the strength and absorbed energy, while the strength and energy were lessened by adhesive failure at the interface, tensile microcleavage at the fibre ends and fibre breakage-induced matrix cracking as well as by the straight fracture path due to fibre alignment in the skin layer in parallel with the notching direction.

Karger–Kocsis and Friedrich [10, 17] suggested K_c of SFRTP as

$$K_c = (m + n R) K_{cm} \quad (3)$$

where K_{cm} is K_c of the matrix, m a matrix stress correction factor, n an energy absorption coefficient, and R the reinforcing effectiveness parameter for characterizing fibre reinforcement in the composite. In composites with a brittle matrix, Equation 3 could be persuasive because m was equal to approximately 1, and n was a positive constant. In the case of a ductile matrix, however, K_c may not be given by a simple linear relationship with R: fracture processes can change with increasing δ, inducing different reinforcing mechanisms ahead of the crack tip; m and n are no longer constant. If R is equivalent to W_f, n for SGFR-PCAE at 23 and 100 °C exhibited rather positive and moderately negative values, respectively, as calculated from the slope in Fig. 4a. A positive value of n resulted from a higher reinforcing effect on the local yielding and failure zone ahead of the ACT than in the case of UR-PCAE, while a negative value was due to microcleavages more readily occurring which caused reduction of the strength. The tensile microcleavage or cracking considerably diminished ductility of the matrix with increasing W_f, as confirmed by the extensive decrease in dimple size measured on the fracture surface of SGFR-PCAE tested at 100 °C (see Fig. 16). The lower ductility influenced the reduction of the absorbed energy, i.e. the deterioration of J_c with W_f as shown in Fig. 4b.

4. Conclusions

Fracture processes of an advanced high-strength thermoplastic PCAE and its SGF composite have been investigated with special attention given to the relationship with the toughness data of K_c and J_c. Test temperatures used were 23 and 100 °C. Reflected and transmitted optical microscopy in combination with scanning electron microscopy were employed in the investigation. UR-PCAE tested at 100 °C revealed large growth of the local plastic yielding zone and formation of numerous tensile microfailures in front of the ACT as compared with the case at 23 °C, causing a substantial improvement in K_c and a great increase in J_c. However, fibre concentration induced both toughening and anti-toughening effects: although fibre spanning and pull-out across the local plastic failure zone and zigzag macroscopic fracture were seen to improve the toughness, adhesive failure at the interface, tensile microcleavage at the fibre ends and straightforward fracture in the skin layer, considerably diminished K_c and J_c, except for the trend of K_c measured at 23 °C. The toughness for SGFR-PCAE may increase with improvement in matrix ductility and interfacial strength, in addition to fibre alignment.

Acknowledgement

The authors thank Mr I. Sugiyama, who is currently at Showa Shell Co., for experimental assistance.

References

1. N. J. JOHNSTON, T. W. TOWELL and P. M. HERGENROTHER, in "Thermoplastic Composite Materials", edited by L. A. Carlsson (Elsevier Science, Amsterdam, 1991) p. 27.
2. N. S. CHOI and K. TAKAHASHI, *Compos. Sci. Technol.* **43** (1992) 237.
3. D. E. SPAHR, K. FRIEDRICH, J. M. SCHULTZ and R. S. BAILEY, *J. Mater. Sci.* **25** (1990) 4427.
4. V. B. GUPTA, R. K. MITTAL and M. GOEL, *Compos. Sci. Technol.* **37** (1990) 353.
5. M. FUJII, N. S. CHOI and K. TAKAHASHI, *Adv. Compos. Mater.* **4** (1994) 47.
6. J. KARGER-KOCSIS and K. FRIEDRICH, *Polymer* **27** (1986) 1753.
7. K. FRIEDRICH, L. A. CARLSSON, J. W. GILLESPIE Jr and J. KARGER-KOCSIS, in "Thermoplastic Composite Materials", edited by L. A. Carlsson (Elsevier Science Publishers, Amsterdam, 1991) p. 233.
8. F. RAMSTEINER and R. THEYSOHN, *Compos. Sci. Technol.* **24** (1985) 231.
9. N. SATO, T. KURAUCHI, S. SATO and O. KAMIGAITO, *J. Compos. Mater.* **22** (1988) 850.
10. J. KARGER-KOCSIS and K. FRIEDRICH, *Compos. Sci. Technol.* **32** (1988) 293.
11. K. TAKAHASHI and N. S. CHOI, *J. Mater. Sci.* **26** (1991) 4648.

12. S. NAGOH, N. S. CHOI and K. TAKAHASHI, *Adv. Compos. Mater.* **3** (1994) 191.
13. Catalogue from Idemitzu Kosan Co. (1992).
14. H. NISHITANI, H. NOGUCHI, Y. H. KIM and T. YAMAGUCHI, *J. Soc. Mater. Sci. Jpn* **41** (1992) 740 (in Japanese).
15. D. P. JONES, D. C. LEACH and D. R. MOORE, *Polymer* **26** (1985) 1385.
16. N. S. CHOI and K. TAKAHASHI, *J. Mater. Sci. Lett.* **12** (1993) 1718.
17. J. KARGER-KOCSIS, in "Application of Fracture Mechanics to Composite Materials", edited by K. Friedrich (Elsevier Science, Amsterdam, 1989) p. 189.
18. W. F. BROWN Jr and J. E. SRAWLEY, *ASTM STP* 410 (American Society for Testing and Materials, Philadelphia, PA, 1966) p. 13.
19. J. R. RICE, P. C. PARIS and J. G. MERKLE, *ASTM STP* 536 (American Society for Testing and Materials, Philadelphia, PA, 1973) p. 231.
20. E. J. KRAMER, in "Crazing in Polymers", edited by H. H. Kausch (Springer, Berlin, 1983) p. 1.
21. D. HULL, in "Polymeric Materials", edited by E. Baer (ASM, Cleveland, OH, 1975) p. 487.
22. N. S. CHOI, K. TAKAHASHI and K. HOSHINO, *NDT E Int.* **25** (1992) 271.
23. A. J. KINLOCH and R. J. YOUNG, "Fracture Behaviour of Polymers" (Applied Science, London, 1983) p. 95.
24. R. WARREN and V. K. SARIN, in "Application of Fracture Mechanics to Composite Materials", edited by K. Friedrich (Elsevier Science Amsterdam, 1989) p. 571.

Received 18 July 1994
and accepted 22 June 1995